Journal of Photochemistry and Photobiology A: Chemistry 225 (2011) 95–105

Contents lists available at SciVerse ScienceDirect

Journal of Photochemistry and Photobiology A: Chemistry

journal homepage: www.elsevier.com/locate/jphotochem

A high-light-harvesting-efficiency of NKX-2593 and NKX-2883 Coumarin dyes in a local electric field: Can a local electric field enhance dye sensitizer solar cells efficiently?

Omolbanin (Setare) Mostajabi Sarhangi, Seyed Majid Hashemianzadeh*, Morteza Moghimi Waskasi, Asqar Pourhassan Harzandi

Molecular Simulation Research Laboratory, Department of Chemistry, Iran University of Science & Technology, Tehran, Iran

ARTICLE INFO

Article history:
Received 2 August 2011
Accepted 2 October 2011
Available online 8 October 2011

Keywords:
Dye-sensitizer solar cell
Time-dependent density functional theory
Coumarin dye
Electric field
Electronic structure
Organic dye

ABSTRACT

The electronic structures and optical absorption spectra of organic dye sensitizers NKX-2593 and NKX-2883 were studied by using density functional theory (DFT), and the vertical excitation energies were calculated within the framework of the time-dependent DFT (TD-DFT) approach both in the gas phase and in ethanol solution. The solvent effects provide changes in both the geometries and the absorption spectra. Electric fields influence any process or transition that involves charge transfer, as a result of Stark effect. Stark spectroscopy is a general expression describing the study of spectral changes in electric fields, and it has been verified to be a broadly functional approach for characterizing the change in dipole moment and polarizability for electronic transitions. The results of this work show that field application, parallel to the dipole moment, can be very effective to increase DSSC efficiency. Our results open the possibility of computationally screening the various predictions on the electronic structure, optical response and in consequence their influences on the efficiency, thus paving the way to an effective molecular engineering of further enhanced sensitizers for solar cell applications.

1. Introduction

Dye sensitizer solar cells are currently attracting extensive academic and commercial interest for the conversion of sunlight energy into electricity, due to their low cost of manufacturing and high rate of efficiency, which is one of the most promising methods for future large-scale power production from renewable energy sources [1–7]. Dye sensitizer solar cells use dye sensitizers to absorb the radiation from the sun and transform the photo excited electron into nanostructured semiconductor electrodes. The most successful sensitizers employed in these cells are polypyridyl ruthenium complexes, which yield photon-to-current power conversion efficiencies of 10–11.18% in standard global air mass 1.5 sunlight [8–10].

As ruthenium is a rare metal and ruthenium-based dye sensitizers lack an absorption band in the long-wavelength region of the solar spectrum, novel dyes without metal or using inexpensive metal are desirable for dye-sensitizer solar cells [11–16]. To further improve the performance of DSSCs, enhancement of the sensitizers' response in all regions of the solar spectrum is to be specially noticed. Recently, more attention has been directed to the application of metal-free organic dyes in DSSCs because of no noble metal resource limitation, relatively facile dye synthesis, easy molecular tailoring and easily tunable absorption properties by suitable molecular design [11,17–22]. Reports of new organic sensitizer design and their performance in DSSCs have been growing in the past years, and promising device efficiencies of up to 9.8% have been demonstrated with a donor–π–acceptor system employing a triphenylamine donor, a binary π-conjugated spacer, and a cyanoacrylic acid acceptor [19,23]. However, the most favorable organic dyes currently deliver only slightly lower efficiencies when employed in DSSC compared to Ru(II) dyes [24].

Metal-free organic dyes used in DSSCs must have an anchoring group (e.g., –COOH and $-SO_3H$) to be adsorbed onto the semiconductor surface with a large electronic coupling. Furthermore, suitable levels for the HOMO and the LUMO of the sensitizer matching the iodine redox potential and the conduction band edge level (E_{cb}) of the TiO_2 electrode are also required. The HOMO level must be more positive than the iodine redox potential, to accept electrons, and to inject electrons, the LUMO level must be more negative than the E_{cb} of the TiO_2 electrode. Thus, the molecular structure of the photosensitizer must be strategically designed for use in dye sensitizer solar cell [25].

Among the metal-free organic dyes studied in DSSCs, Coumarin derivatives have been intensively studied, both experimentally and

* Corresponding author. Tel.: +98 21 77240287; fax: +98 21 77491204.
E-mail addresses: hashemianzadeh@yahoo.com, hashemianzadeh@iust.ac.ir (S.M. Hashemianzadeh).

1010-6030/$ – see front matter © 2011 Elsevier B.V. All rights reserved.
doi:10.1016/j.jphotochem.2011.10.004

theoretically, and are one of the most promising dyes [26–32]. On the basis of the concept of donor–π conjugation bridge–acceptor structure, Hara et al. synthesized a series of Coumarin dyes (NKX-2593 and NKX-2883) [25,33,34] by inserting various numbers of thiophene or methine moieties as π bridge between Coumarin as electron donor and cyano carboxylic acid as electron acceptor. Due to the narrow absorption area in the visible region, wide absorption range in the visible region for the Coumarin dye is required to attain a solar-energy to electricity conversion with high efficiency. Therefore, the absorption spectra of Coumarin dyes must be broadened and red-shifted for more efficient solar-cell performance in terms of harvesting sunlight. The absorption spectra of Coumarin dyes could be red-shifted by expansion of the π conjugation in the dyes and introduction of electron-donating and -withdrawing substituents into the dye framework; such substituents can shift the levels of the dyes' highest occupied molecular orbitals (HOMOs) and their lowest unoccupied molecular orbitals (LUMOs) [25,29,32].

Theoretical calculations are useful not only in the description of DSSC properties, but also in the design of new higher performance sensitizers manufactured by a change in their structure and/or physical properties such as temperature, solvent, and external electric field [35]. The change in the structure can be achieved by adding or substituting various substituents. Such design investigations have become possible only lately, and they take an important step toward the optimization of DSSC dyes, by means of effective and accurate modeling of their ground-state properties, together with a reliable description of their excited states. Large-scale quantum mechanical calculations, able to precisely predict the electronic and spectroscopic characteristics of the dyes, would be a really powerful and comparably low cost device in the beforehand design of novel and greatly efficient sensitizers [36].

In this paper, the molecular structure and the electronic properties of the ground and lowest π–π^* excited states for a series of Coumarin derivatives, NKX-2593 and NKX-2883, are studied. The reported Coumarin dyes absorb light weakly over 700 nm, and little success was achieved to extend photo response to the longer wavelength region. Therefore, efficiently harvesting incident photons in the longer wavelength region still remains a big challenge for Coumarin dyes. A lot of researches have been conducted to remove the problem. The most notable ones include using dye mixtures [37] and investigating substituent effects [25].

Our suggestion in the current paper to overcome this challenge is applying an external electric field. Local electric fields could lead to a change in the absorption spectrum due to the Stark effect. Such electric fields acting on ground-state dye molecules can red-shift the absorption peak of the dye by lowering the energy gap between the highest occupied molecular orbitals (HOMOs) and the lowest unoccupied molecular orbitals (LUMOs). It can be strongly mentioned that the applied field led to a red-shift for DSSCs, and, to our surprise, there was a striking increase in the absorption coefficient.

2. Computational methods

All sensitizers were optimized by the use of density-functional theory (DFT) calculations. The DFT was treated according to Becke's three parameter gradient-corrected exchange potential, Lee–Yang–Parr gradient-corrected correlation potential (B3LYP) and the standard 6-311G (d) basis set [38–41]. The excitation energies and oscillator strengths for the two dyes at the optimized geometry in the ground state were obtained in the framework of TD-DFT calculations with the hybrid functional B3LYP, PBE1PBE, MPW1PW91 and the 6-311G (d) basis sets [42–46]. The 30 lowest singlet–singlet excitation energies were considered in those calculations. The electronic absorption spectrum requires calculation of the allowed excitations and oscillator strengths. The solvent effects were evaluated using the non-equilibrium implementation of the conductor-like polarizable continuum model (CPCM) [47]. Solvent could affect the geometry, electronic structures and the related properties of molecule. In this work we also present the changes of the electronic structure and optical properties induced by an external electric field. Optimization calculations were carried out with and without an applied electric field. Eight different fields of 5, 10, 15, . . ., 40×10^{-4} a.u., parallel to the dipole moment, were applied on the dyes and their geometry in each field was then optimized by DFT, B3LYP and the 6-311G (d) basis set. All chemical quantum calculations were carried out with the Gaussian03 program package [48].

Excitation energy calculations on the optimized sensitizer were later carried out in the corresponding electric fields at the same level of theory. The electric field term is included in the Hamiltonian and results in a change in the energy of both occupied and unoccupied levels which in situ results in a shift of transition energies.

To understand the nature and magnitude of the intramolecular resonance over the different parts of the dyes and to calculate the NBO conjugation stabilization energies, the natural bond orbital (NBO) theory was conducted on optimized geometries. NBO calculations were performed using the program packages of NBO5.0 [49].

3. Results and discussion

For a proper discussion and comparison of theoretical results, it is important to have a clear picture of our theoretical data. All of the calculations were conducted by B3LYP/6-311G (d), MPW1PW91/6-311G (d) and PBE1PBE/6-311G (d) methods. The calculated results obtained at the MPW1PW91/6-311G (d) and PBE1PBE/6-311G (d) levels were very close to each other. For clarity, the results of MPW1PW91/6-311G (d) will be used in the discussion unless otherwise stated. In this section, we present results for NKX-2593 and NKX-2883, organized in the following manner. We first study, in detail, the electronic structure of these two dyes in gas phase and solvent. We then compare various theoretical methods for the description of the ground and excited-state electronic excitation energies at the equilibrium geometry for NKX-2593 and NKX-2883. Following this, we investigate the absorption spectra and electronic excitations between ground and excited states in the presence and absence of solvent effects. Next, the electronic structure, absorption spectra and excitation energy between ground and excited states are analyzed in the presence of an applied electric field for NKX-2593 and NKX-2883. Finally, we interpret and analyze the resulted data.

3.1. Electronic structure

We analyzed the electronic structure of both organic sensitizers in vacuum and in ethanol solution, which is the solvent used to record the experimental spectra. A schematic representation of the molecular orbital energies and isodensity plots of the frontier molecular orbitals of NKX-2593 and NKX-2883 is reported in Fig. 1.

The highest occupied molecular orbital (HOMO) of NKX-2593 and NKX-2883, both in vacuum and in solution, is delocalized over the cyano-(thiophen) acrylic acid, with sizable components from the cyano- and carboxylic moieties. On the other hand, the HOMO−1 is a π-bonding orbital delocalized over the entire molecule, with maximum components on the thiophene and cyanoacrylic moieties. The lowest unoccupied molecular orbital (LUMO) is for both sensitizers a π^* orbital delocalized throughout the Coumarin moiety. The HOMO energy levels for NKX-2593 and

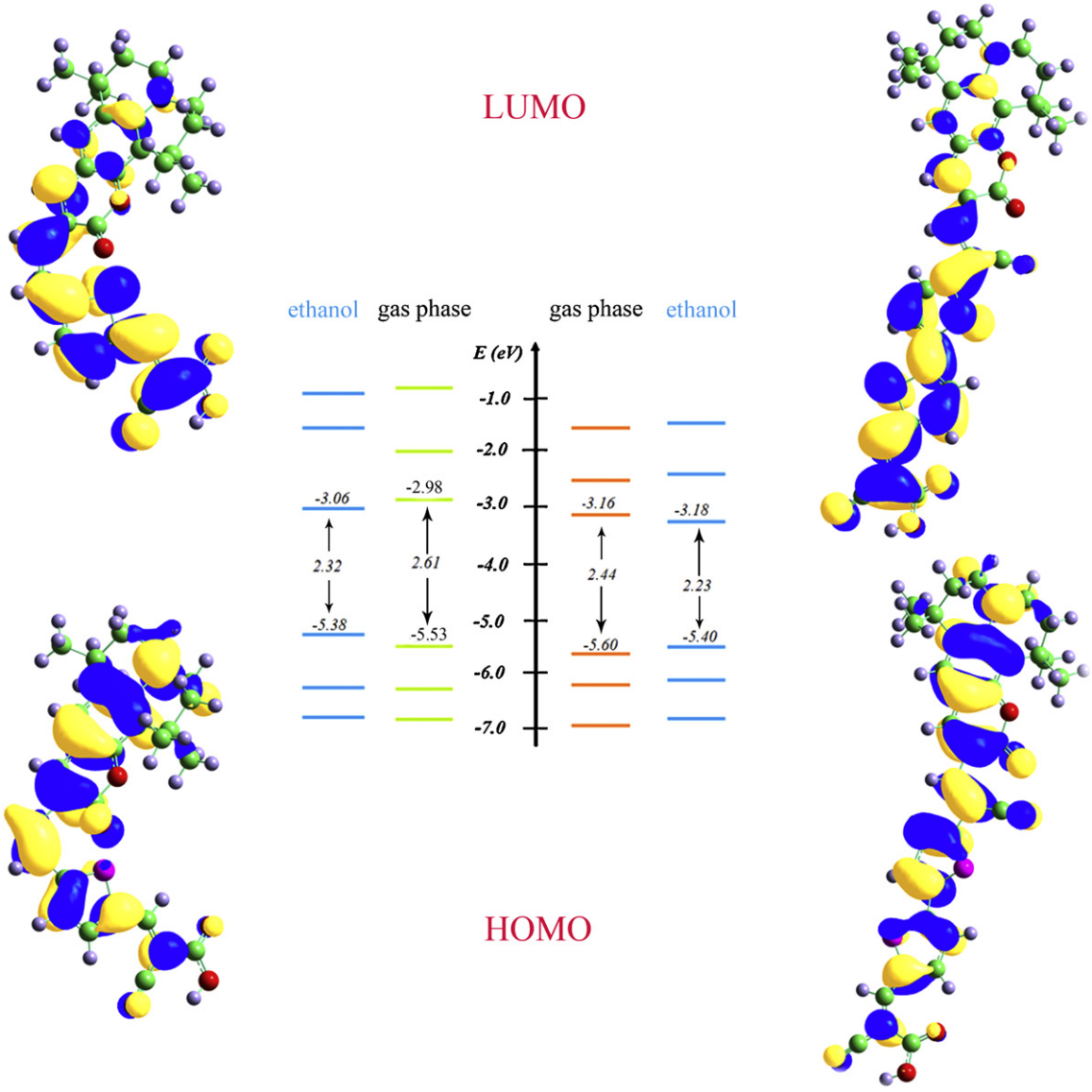

Fig. 1. Frontier molecular orbitals of NKX-2593 (left) and NKX-2883 (right) sensitizers calculated at the B3LYP/6-311G (d) level in the gas-phase.

NKX-2883 in gas phase are −5.538 and −5.597 eV and their corresponding LUMO energy levels are −2.298 and −3.158, respectively. It is remarkable to notice that the HOMO and LUMO of NKX-2883 are stabilized by 0.06 and 0.86 eV, respectively, as compared to the corresponding NKX-2593 orbitals. As a result, the NKX-2883 HOMO–LUMO gap reduces to 2.44 eV, as compared to 2.61 eV calculated for NKX-2593, with the sizable LUMO stabilization due to the increased conjugation along the substitutes owing to the presence of a CN-group and thiophene units. Inclusion of solvent effects does not lead to a qualitative change in the electronic structure picture discussed above, even though, for both dyes, as a result of HOMO unstabilization and LUMO stabilization in solution, smaller HOMO–LUMO gaps are calculated as compared to the gas phase. We notice that the trend of calculated HOMO–LUMO gaps is nicely in accord with the spectroscopic data, showing a red-shift of the absorption maximum in going from NKX-2593 to NKX-2883.

To have a better insight into the nature and strength of the intramolecular resonance between the different parts of the molecule, particularly acceptor and donor moieties, for NKX-2593 and NKX-2883 dyes, NBO analysis was conducted. Here, we employ NBO methods to evaluate the strength of π-conjugation of the dyes by the natural bond orbital (NBO) second order perturbation stabilization energies.

The role of electronic delocalization can be quantitatively evaluated by using the NBO procedure. The directly estimated approach of π-conjugative stable energies using NBO second order perturbation analysis will be very helpful to analyze the π-conjugation strength of NKX-2593 and NKX-2883. We evaluate the π-conjugation stabilization strength by NBO donor–acceptor interaction energies. The NBO donor–acceptor interaction energies are calculated on the basis of Lewis- and Pauling-like localized structural and hybridization theories and are presented with the classical π-conjugation concepts by a refinement of NBO analysis. This interaction energy corresponds to the charge delocalization due to the loss of electronic occupation from the localized Lewis molecular orbital to the non-Lewis molecular orbital leading to the distribution of electronic charge and therefore the perturbation from idealized Lewis structure description.

For a characteristic conjugated π-bond network with two pairs of conjugated π bonds, the delocalized molecular orbitals can be pictured using the refined idealized Lewis structures by NBO donor–acceptor interaction of $\pi_a \rightarrow \pi_b^*$ and $\pi_a \rightarrow \pi_b^*$. According

to the perturbation theory, the lowering energy due to $\pi_a \rightarrow \pi_b^*$ interaction, which is also referred to as the quantum mechanical resonance energy (denoted as QMRE), is estimated as

$$\Delta E(\pi_a \rightarrow \pi_b^*) = -q_a \frac{\langle \pi_a | \hat{f} | \pi_b^* \rangle}{\Delta \varepsilon} \quad (1)$$

where q_a is the ath donor orbital occupancy and $\Delta\varepsilon = \varepsilon_b - \varepsilon_a$ is the energy difference of interacting NBOs and the matrix element $\langle \pi_a | \hat{F} | \pi_b^* \rangle$ is the off-diagonal element associated with the NBO Fock matrix. The strength of π-type conjugation and its variations by introducing resonance moieties can be conveniently visualized in terms of the NBO second order perturbation stabilization energies $\Delta E(\pi_a \rightarrow \pi_b^*)$ and the charge transfer from π_a to π_b^*. The sum of stabilization energies, that is, $\Delta E\pi_a \rightarrow \pi_b^* + \Delta E\pi_b \rightarrow \pi_a^*$ is chosen as an indicator of the degree of the π-conjugation. As mentioned above, to prove the reliability of QMRE as a criterion of π-conjugative strength, we studied the change of π-conjugation due to the introduction of conjugated functional groups and changes in physical properties. According to NBO donor–acceptor interaction theory, the charge occupancy of the π^* NBO also indicates the strength of π-conjugation [50–52].

The QMRE sums drastically rise up with the π-conjugation increase from NKX-2593 to NKX-2883. The stabilization energies corresponding to second order perturbation energy are 2007.21 and 2461 kcal/mol in gas phase and 2027 and 2467 kcal/mol in solution for NKX-2593 and NKX-2883, respectively. As it can be easily observed, as a result of the introduction of CN and thiophene to the dye NKX-2883 there is an increased resonance and stabilization in the molecule, verified by QMRE corresponding to second order perturbation.

3.2. Electronic excitations and absorption spectra

In experimental studies of Hara et al., because of the presence of extra CN and thiophene moieties in NKX-2883, it showed absorption band in 552 nm, which considerably red-shifted compared to that of NKX-2593 lying in 510 nm. To gain insight into the excited states, TD-DFT excited state calculations using three kinds of hybrid functional B3LYP, MPW1PW91, and PBE1PBE and 6-311G (d) basis set are carried out on the 30 lowest spin-allowed singlet–singlet transitions for NKX-2593 and NKX-2883 dyes in vacuum and solvent [53]. The TD-DFT simulated absorption spectra of the Coumarin NKX-2593 and NKX-2883 are indicated in Fig. 2. The top panel shows the spectra calculated in the gas phase, and the lower one shows the spectra obtained in ethanol solution. The contributions of the excited state configurations to all transitions were calculated using SWizard program [54].

As it can be observed in Fig. 2, compared with the results of experiment, the results of TD-DFT in solvent are consistent with experimental data. By comparing the experimental spectrum with the calculated absorption spectrum of the NKX-2593 and NKX-2883 in ethanol solution, we notice that there is a good agreement between theory and experiment both in terms of band positions and relative intensity. It is strongly to be noted that the calculated oscillator strengths of molecular orbital transitions do not always match the experimental absorbance, the relative intensities of the absorption bands for these compounds are capable of being used as only a qualitative reference rather than a quantitative index. Computed vertical energy gaps in the gas phase and ethanol, obtained by the use of three kinds of hybrid functional B3LYP, MPW1PW91, and PBE1PBE, are shown and compared to experimental absorption band maxima in ethanol solution in Table 1.

Compared with experimental data, the results of the calculations imply that the hybrid functional PBE1PBE and MPW1PW91 are more suitable than B3LYP for calculating electronic absorption spectra of Coumarin dyes NKX-2593 and NKX-2883 [55]. Since there is not a major difference in the gained results for the hybrid functional PBE1PBE and MPW1PW91 for the two dyes applied in this paper, the hybrid functional MPW1PW91 is used.

NKX-2593 and NKX-2883 showed a maximum absorption in gas phase at 507.9 and 532.90 nm, respectively. These two peaks correspond to the lowest-energy excitation from HOMO to LUMO. The lowest transitions for NKX-2593 and NKX-2883 were calculated in gas phase at 2.87 eV and 2.69 eV, respectively, corresponding to a charge-transfer (CT) excitation from the aniline-based HOMO to the LUMO localized on the thiophene–cyanoacrylate moieties.

The wavelengths, oscillator strengths, transition energies and molecular orbital excitations for the most relevant transitions of NKX-2593 and NKX-2883 were obtained through TD-DFT calculations in ethanol, which was often used as solvent in previous experimental research works. The solvent–solute interaction has been included at the structural level through geometry optimization of NKX-2593 and NKX-2883 dyes within the CPCM model, and also at the electronic structure level, incorporating the environment effects in the computation of the ground and excited states. Calculated maximum absorptions in ethanol solution, compared to the gas phase, show a red-shift in all methods. For the dye NKX-2593 calculated in ethanol solution, the maximum absorption peak of the spectrum appears at 582.93 nm, a 75-nm red shift from the gas-phase spectrum. And for NKX-2883, calculated by the CPCM model, in ethanol solution, the maximum absorption peak turned out to be at 596.99, showing a red-shift of 64 nm. There was an increase observed in the oscillator strength of the lowest-energy excitation from 1.7236 to 1.7510.

Since the absorption band in visible and near-UV region is the most important region for photo-to-current conversion, only the singlet–singlet transitions of the absorption bands with the wavelength longer than 300 nm, and transition energies in gas and solvent phases are listed in Table 2.

As shown in Table 2, for example, there is an absorption band for NKX-2593 in 391.7 nm, in the gas phase, which is a mixture of HOMO−1 → LUMO (58%) and HOMO → LUMO+1 (41%) transitions with oscillator strength of 0.4212, whereas, for NKX-2883 the absorption band is found in 433.2 nm, a mixture of HOMO → LUMO+1 (62%) and HOMO−1 → LUMO (35%) transitions with oscillator strength of 0.5644.

TD-DFT can be an appropriate method to calculate maximum absorption and oscillator strength. So, new structures can be suggested and we can then theoretically investigate how maximum absorption and oscillator strength increase can affect their efficiency.

3.3. Electric fields and the dyes

Coumarin dyes have a trivial absorption in long wavelengths and little success has been achieved to promote their photon-to-current respond. Besides, these dyes show a narrow absorption peak, which is regarded as one of their prominent disadvantages. One of the essential factors to increase the efficiency of dye sensitizer solar cells is to broaden and red-shift their absorption bands. To do this, a lot of attempts, such as a π-conjugation increase by adding methine, thiophene and cyanide moieties, have been done [25]. Enhancement of maximum absorption oscillator strength, broadening their peaks and their red-shift are factors of importance in increasing the dye sensitizer solar cell efficiency, which still remains as a big challenge. To observe whether local electric field can broaden and red-shift maximum absorption peaks, in the current study, electric fields of different strength, 5, 10, ..., 40×10^{-4} a.u., parallel to the dye dipole moment were applied. The excitation energy in the presence of static external electric field depends on the changes in dipole moment and polarizability during excitation process. Local fields change the transition moment between ground and excited

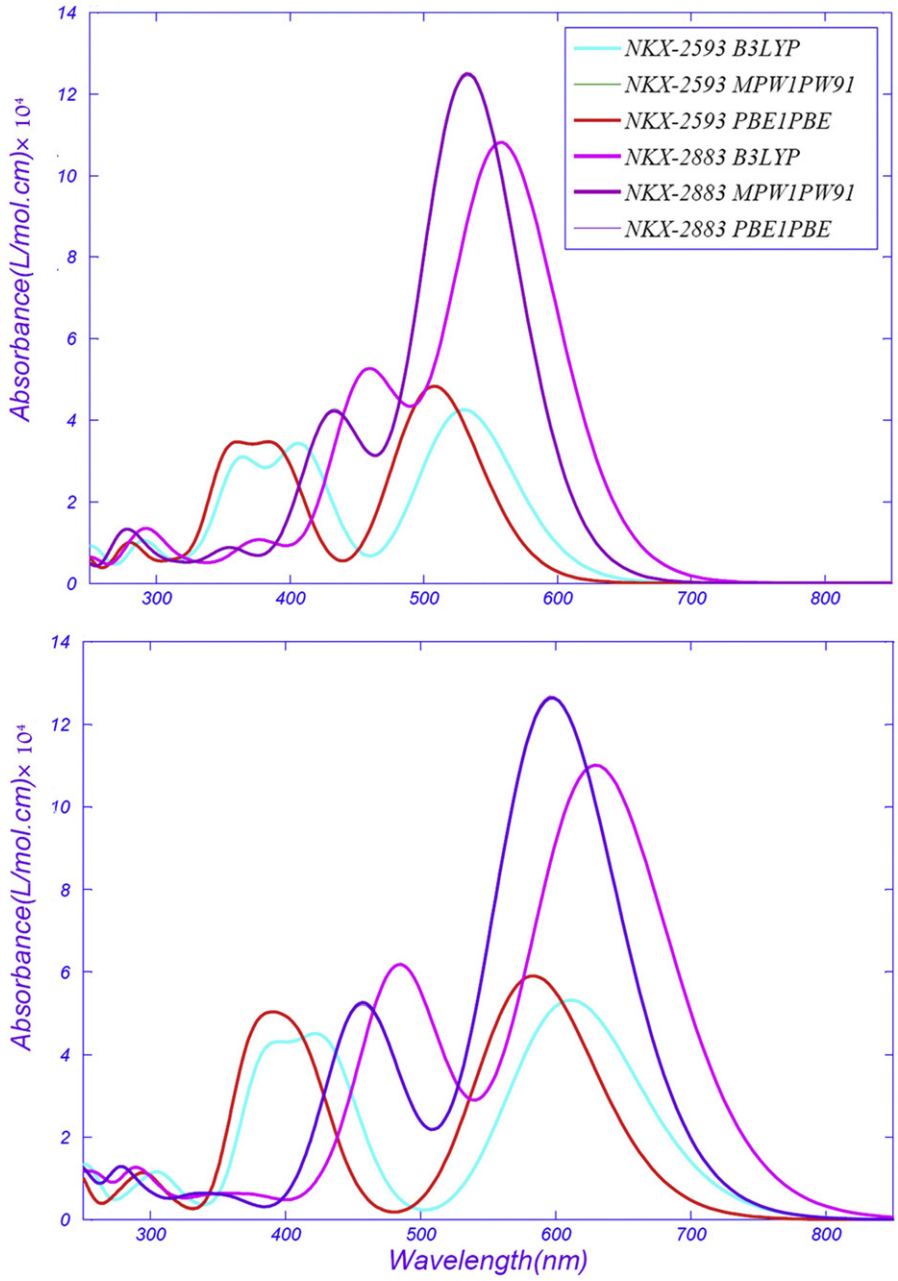

Fig. 2. Simulated absorption spectra of NKX-2593 and NKX-2883 in the gas phase (top) and ethanol solution (bottom) calculated by TD-DFT at the three kinds of hybrid functional B3LYP, MPW1PW91, and PBE1PBE/6-311G (d) levels (there is not a difference in the gained results for the hybrid functional PBE1PBE and MPW1PW91 and their bands overlay each other).

states and, therefore, affect the transition allowance and strength. The results show that the dipole moment of the dye increases by increasing local field in the same direction. Application of local electric fields and changing the strength of the applied fields influence the absorption spectrum, due to Stark effect [56].

Stark spectroscopy is a general expression describing the study of spectral changes in electric fields, and it has been verified to be a broadly functional approach for characterizing the change in dipole moment and polarizability for electronic transitions. A change in dipole moment causes a linear dependence on the applied electric

Table 1
Maximums of absorption spectra (λ_{max}) of NKX-2593 and NKX-2883 in the gas phase and ethanol solution calculated by TD-DFT at the three kinds of hybrid functional B3LYP, MPW1PW91, and PBE1PBE/6-311G (d) levels and their comparison with experimental data.

	TD-DFT						
	Gas phase			Ethanol solution			
Dye	B3LYP	PBE1PBE	MPW1PW91	B3LYP	PBE1PBE	MPW1PW91	Expe
NKX-2593	530.05	508.11	507.85	611.21	583.30	582.93	510
NKX-2883	558.14	532.93	532.90	629.77	597.37	596.99	552

Table 2
Selected excitation energies (nm) and oscillator strengths for the optical transitions between 350 and 600 nm of the absorption spectra of the NKX-2593 and NKX-2883 sensitizers calculated by TD-DFT at the MPW1PW91/6-311G (d) level.

Gas phase			Ethanol solution		
E	*f*	Composition	*E*	*f*	Composition
		NKX-2593			
507.9	0.6672	H → L (+99%)	582.9	0.8166	H → L (+99%)
391.7	0.4212	H−1 → L (+58%) H → L+1 (41%)	412.0	0.5160	H−1 → L (+63%) H → L+1 (36%)
354.6	0.0655	H−2 → L (+84%) H → L+1 (+6%)	375.7	0.5408	H → L+1 (+62%) H−1 → L (+36%)
353.5	0.3542	H → L+1 (+50%) H−1 → L (+36%) H−2 → L (10%)	371.5	0.0025	H−2 → L (+96%)
316.0	0.0599	H−1 → L+1 (+71%) H−3 → L (+22%)	318.4	0.0345	H−3 → L (+59%) H−1 → L+1 (+30%) H−4 → L (+9%)
		NKX-2883			
523.9	1.7236	H → L (+98%)	597.0	1.7510	H → L (+97%)
433.2	0.5644	H → L+1 (+62%) H−1 → L (35%)	459.4	0.6678	H → L+1 (+64%) H−1 → L (32%)
397.0	0.0519	H−1 → L (+64%) H → L+1 (+35%)	427.3	0.1070	H−1 → L (+66%) H → L+1 (+34%)
355.9	0.0839	H−1 → L+1 (+80%) H−2 → L (+11%)	362.7	0.0082	H−2 → L (+58%) H−2 → L+1 (+28%) H−2 → L+1 (+11%)
352.8	0.0280	H−2 → L (67%) H−2 → L+1 (+16%) H−1 → L+1 (11%)	362.2	0.0499	H−1 → L+1 (+62%) H−2 → L (23%) H−2 → L+1 (6%)

field while a change in polarizability gives a quadratic field dependence of the excitation energy [57–62]. The change in transition frequency resulted by an external electric field is given by [63]

$$\Delta\nu = -\Delta\vec{\mu}.\vec{E} - \frac{1}{2}\vec{E}.\underline{\Delta\alpha}.\vec{E} \quad (2)$$

where $\Delta\vec{\mu}$ is the change in dipole moment and $\underline{\Delta\alpha}$ is the change in polarizability between the ground and excited states of the molecule. From Eq. (2), one distinguishes first- and second order Stark effects, which are, respectively, linear and quadratic in the electric field.

Excitation energy (λ_{max}) between the ground and excited states in the presence of electric fields of different strength of 5, 10, 15, ..., 40×10^{-4} a.u. was plotted versus electric field strength. The data were then fitted with the equation $Y = aX^2 + bX + c$ with a well acceptable regression coefficient. By the use of this equation, the change in dipole moment and polarizability between ground and excited states can be simply calculated. $\Delta\vec{\mu}$ and $\underline{\Delta\alpha}$ were calculated to be 12.32 Debye and 319.95 a.u. for NKX-2593, which were extracted from equation $Y = -2.638 \times 10^{-39}X^2 - 4.11 \times 10^{-29}X + 3.93 \times 10^{-19}$ with a regression coefficient of 0.999 and the same values for NKX-2883, upon the calculations, were found to be 3.1 Debye and 345.88 a.u., respectively for dipole moment and polarizability, extracted from equation $Y = -2.027 \times 10^{-39}X^2 - 1.034 \times 10^{-29}X + 3.75 \times 10^{-19}$ with a regression coefficient of 0.998. Since the change in dipole moment and polarizabilty between ground and excited states can be determined by other methods [62,64], for each other system it is possible to evaluate frequency changes upon using given data for $\Delta\vec{\mu}$ and $\underline{\Delta\alpha}$ and putting the different values for field strength in Eq. (2). These kinds of evaluations can be expanded to spectral studies of other sensitizers.

3.3.1. Electronic structures in local electric fields

Electric fields affect any process or transition that involves the movement of charge, as a result of Stark effect. Electronic structure analysis was conducted for both sensitizers in the local electric field of 10×10^{-4} a.u. HOMO energy, in gas phase and the local electric field of 10×10^{-4} a.u., is −5.48 for NKX-2593 and −5.51 eV for NKX-2883, which is unstabilized, compared to the off-field condition, by values of 0.107 and 0.225 eV respectively. Also, the calculated energies for LUMO in the presence and absence of the local field are respectively −3.03 and −2.93 eV for NKX-2593 and −3.38 and −3.16 eV for NKX-2883. As it can be simply understood, the reduction of the HOMO–LUMO gap is basically due to stabilization of the LUMO energy in presence of a local electric field. Also, the influences of the field on these two dyes in ethanol solution were investigated. HOMO energy level for NKX-2593 and NKX-2883 in ethanol solution is stabilized by the value of 0.17 and 0.23, respectively, compared to the gas phase. And, LUMO energy level stabilization in the same condition is 0.2 and 0.1 eV, therefore, the energy gap in solvent phase is reduced, compared to the gas phase.

It is clear that local electric field in the presence of a solvent leads to more red-shift than it does in gas phase, which is due to solvent effect. In solution, sensitizers are also affected by the change in polarizability since the electric field of the surrounding solvent induces a dipole moment of a different size. Changes in dipole moment alter the dye–solvent electrostatic interaction in the ground and excited states, which causes a shift in the absorption maximum.

According to the second order perturbation theory, local field can increase energy stabilization. The stabilization energies corresponding to second order perturbation energy, in the presence of local electric field, are 2046.08 and 2470 kcal/mol in gas phase and 2397 and 2490 kcal/mol in solution for NKX-2593 and NKX-2883, respectively. As it can be easily observed, as a result of the local field application to the dyes there is an increased resonance and subsequently an increased stabilization in the molecule, compared to off-field condition, verified by QMRE corresponding to second order perturbation.

Changing the dye structure by introducing various functional groups to increase delocalization, and hence DSSCs' efficiency, is reported in a lot of studies. Our results indicate that the same improvement can be simply achieved by applying an electric field of proper strength.

3.3.2. Electronic excitations and absorption spectra in local electric fields

As it is previously shown, TD-DFT method can well predict absorption spectra (λ), oscillator strength and therefore the efficiency of dye sensitizer solar cell. Therefore, we utilized this method to study the effects of the local electric field on the dye sensitizer solar cell efficiency. To have a better insight of excited state electronic transitions in the presence of an electric field, TD-DFT calculations using hybrid functional MPW1PW91 and 6-311G (d) basis set were accomplished for 30 lowest transitions.

Orientation of local electric field is one of the most important factors in applying an electric field on the dye. We calculated possible orientations of NKX-2593 and NKX-2883 in the presence of local electric field. In the current study an electric field of the strength of 10×10^{-4} a.u. parallel and antiparallel to the dipole moment of the dye was applied to discover the optimum orientation for the electric field. To do so, TD-DFT calculations were carried out to obtain the absorption spectrum in the local electric field. The results obtained from TD-DFT calculations indicate that the application of an electric field parallel to the dipole moment of the dye results in an incredible increase in the dipole moment of the dye, consequently influencing the absorption spectra. The dye NKX-2593, in the local electric field of 10×10^{-4} a.u. parallel to its dipole moment, showed a dipole moment of 15.7 Debye and a maximum peak at 531 nm. But the values for off-field condition are 12 Debye and 507 nm for dipole moment and maximum peak, respectively. For the NKX-2883, we observed that a local field of 10×10^{-4} a.u. parallel to the dipole moment increased the dipole moment from 17.86, in the absence of the field, to 22.5, on the local field. Also, the maximum absorption shifted from 532 nm, in the off-field condition, to 601 nm, on the local field. But the application of a local electric field anti-parallel to the orientation of the dipole moment of these two sensitizers resulted in a decrease in the dipole moment, compared to the off-field condition, and consequently blue-shifted the maximum absorption. For instance, for the NKX-2593 dye, the dipole moment and maximum absorption reduced to 11.6 Debye and 484 nm, respectively. The application of an anti-parallel local field of 10×10^{-4} a.u. on NKX-2883 reduced the dipole moment from 17.86, in off-field condition, to 15.73, on the local field, and the maximum absorption underwent a blue-shift of 14 nm. The obtained results for these two dyes, in parallel and anti-parallel local electric fields of 10×10^{-4} a.u. and in gas phase, are illustrated in Fig. 3.

According to these results, local fields parallel to the dipole moment of the dyes are in favor of our goal in this paper to promote the efficiency of the dyes in dye sensitizer solar cells. HOMO and LUMO energy levels and the energy gap between them in various electric fields are illustrated in Fig. 4. As it is clear, the gap decreases by increasing electric field strength. But how does the local electric field, parallel to the dipole moment, induce such a decrease in the energy gap of the dyes?

We used TD-DFT calculations, to answer this question. The results show that the local electric field, whether parallel or anti-parallel to the dipole moment, has no big effect on HOMO energy levels of the dyes and just unstable them in a very trivial amount, but it has the most influences on the LUMO energy levels of the dyes. The local electric field parallel to the dipole moment of the dye made LUMO of NKX-2593 and NKX-2883 stable by the values of 0.11 eV and 0.22 eV, respectively.

As an example, the singlet–singlet transitions of the absorption bands with the wavelength over 300 nm, and transition energies in gas and solvent phases, for the field of 5×10^{-4} a.u., are listed in Table 3 (See Supporting information). As it is clear from Table 3, the NKX-2593 on the local electric field of 5×10^{-4} a.u. shows a maximum absorption peak at 517.7 nm with the oscillator strength of 0.7963, corresponding to electronic transitions from HOMO to

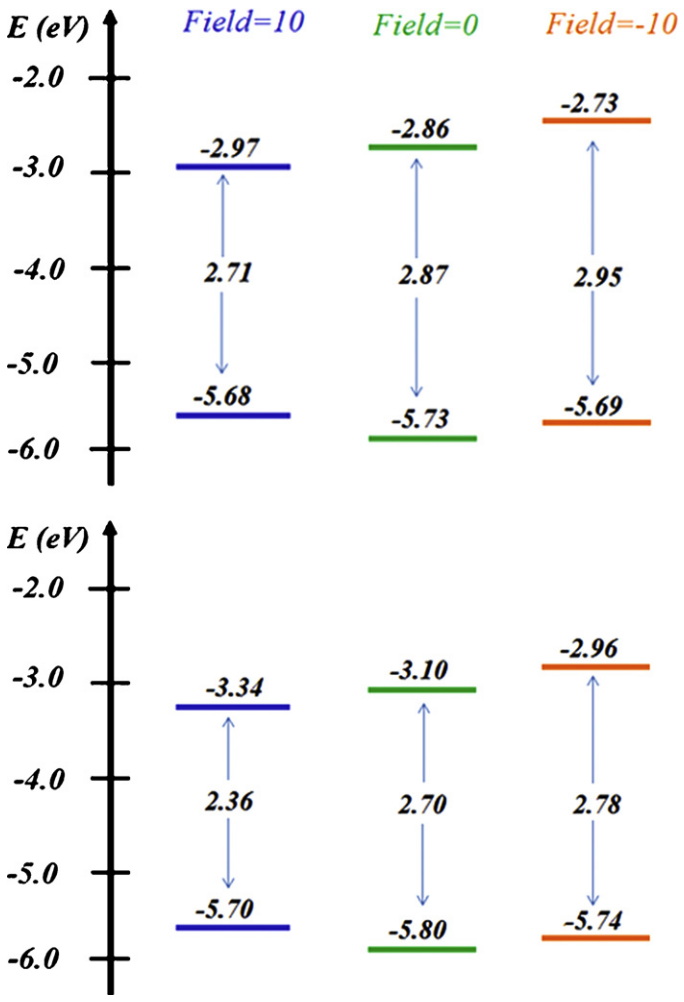

Fig. 3. Schematic representation of the frontier molecular orbitals of NKX-2593 (top) and NKX-2883 (bottom) in gas phase and presence of an electric field of 10×10^{-4} a.u., parallel and anti-parallel to the dipole moment, calculated by TD-DFT at the MPW1PW91/6-311G (d) level.

LUMO. Compared to the off-field condition, there is a red shift of 10 nm and the oscillator strength is increased by the amount of 0.11.

For the dye NKX-2883 in the same local field, the maximum absorption peak was found to be at 563.9 nm with oscillator strength of 1.47, while these values in the absence of the local electric field are respectively 532 nm and 1.7. Although the oscillator strength for NKX-2883 is decreased, an increase in the efficiency is observed, which will be later discussed in detail. Simulated absorption spectra of NKX-2593 and NKX-2883 in the gas phase, ethanol solution and presence of various electric field strengths are illustrated in Fig. 5. To get the most compatibility with the experimental conditions and have an acceptable understanding over electronic transitions, TD-DFT calculations were done in ethanol, as a solvent, and in the local electric field. Calculations in the solvent phase and presence of an electric field for NKX-2593 and NKX-2883 show that the shift of the maximum absorption to longer wavelengths has increased. Generally, a similar trend to the gas phase calculations as a result of electric field enhancement is observable.

As it can be simply deduced from the data in Fig. 5, the red shift and oscillation strength growth increase by increasing electric field strength. However, it should be noticed that oscillator strength up to fields of 20 a.u. is less than that for off-field condition and at 20 a.u. it approximately equals to its off-field value and then

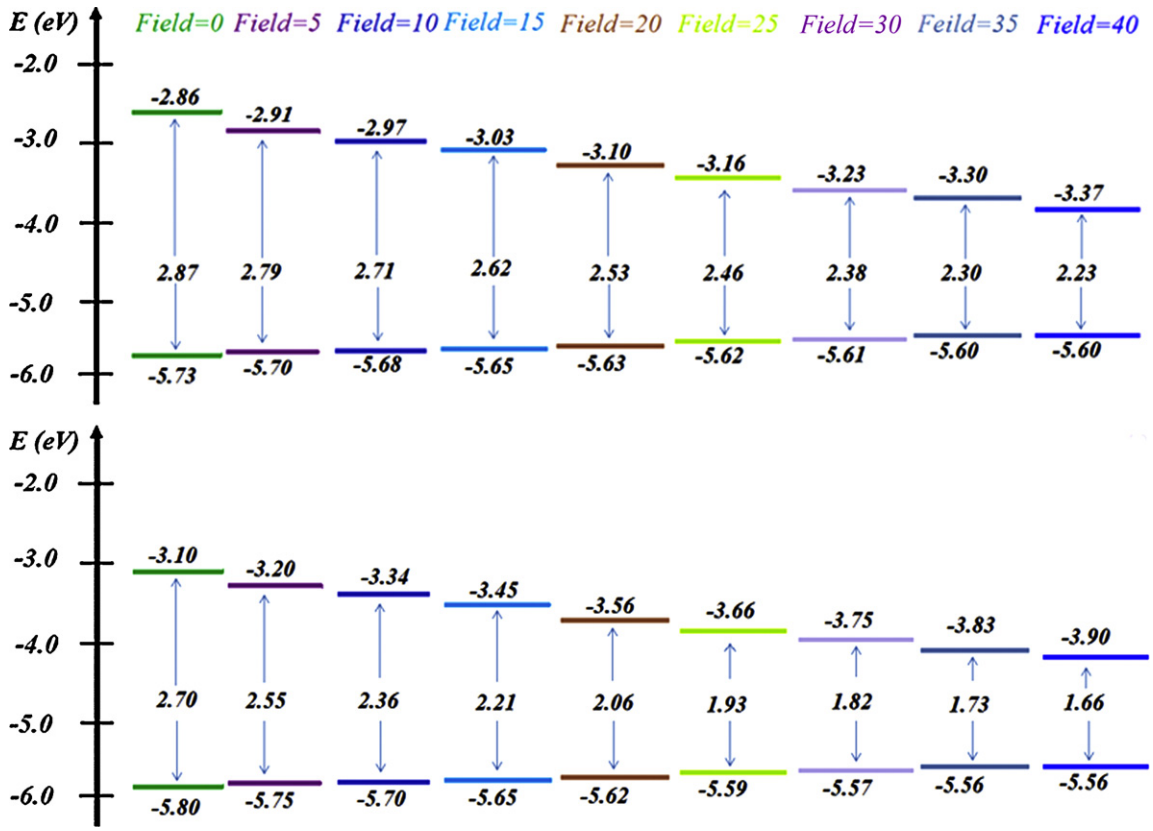

Fig. 4. Schematic representation of the frontier molecular orbitals of NKX-2593 (top) and NKX-2883 (bottom) in gas phase and nine different electric field ($\times 10^{-4}$ a.u.).

increases with increasing electric field strength. The maximum absorption and oscillator strength obtained in the local electric field show that a local electric field causes a remarkable broadening and red-shift in the absorption bands. The broadening of the peaks in the presence of local electric fields is far too vivid and the corresponding spectrums are illustrated in Fig. 5, but for a quantitative analysis, the Peak Area for these two dyes in different local fields has been calculated and listed in Table 4. For these two dyes, the Peak Area is calculated through following equation,

$$\%A = \frac{A - A_{ref}}{A_{ref}} \tag{3}$$

Table 3
Selected excitation energies (nm) and oscillator strengths for the optical transitions between 350 and 700 nm of the absorption spectra of the NKX-2593 and NKX-2883 sensitizers at the MPW1PW91/6-311G (d) level and in an electric field of 5×10^{-4} a.u.

Gas phase			Ethanol solution		
E	*f*	Composition	*E*	*f*	Composition
		NKX-2593			
517.7	0.7963	H → L (100%)	611.0	0.9238	H → L (100%)
393.9	0.4010	H−1 → L (+59%) H → L+1 (40%)	419.6	0.5102	H−1 → L (+64%) H → L+1 (35%)
360.7	0.0010	H−2 → L (+94%)	384.0	0.0028	H−2 → L (+96%)
354.2	0.3886	H → L+1 (+57%) H−1 → L (+39%)	378.2	0.5206	H → L+1 (+62%) H−1 → L (+35%)
315.3	0.0613	H−3 → L (+55%) H−1 → L+1 (+40%)	320.3	0.0252	H−3 → L (+63%) H → L+1 (+14%) H−4 → L (+19%)
		NKX-2883			
563.9	1.4743	H → L (+99%)	654.5	1.5989	H → L (+98%)
444.7	0.9139	H → L+1 (+59%) H−1 → L (39%)	480.5	1.1103	H → L+1 (+58%) H−1 → L (39%)
404.0	0.0391	H−1 → L (+60%) H → L+1 (+39%)	438.0	0.0361	H−1 → L (+59%) H → L+1 (+40%)
365.9	0.0050	H−1 → L+1 (+14%) H−2 → L (+84%)	383.6	0.0077	H−2 → L (+89%) H−2 → L+1 (+10%)
355.9	0.0352	H−1 → L+1 (86%) H−3 → L (+6%)	361.3	0.0040	H−1 → L+1 (+81%) H → L+2 (8%) H−3 → L (8%)

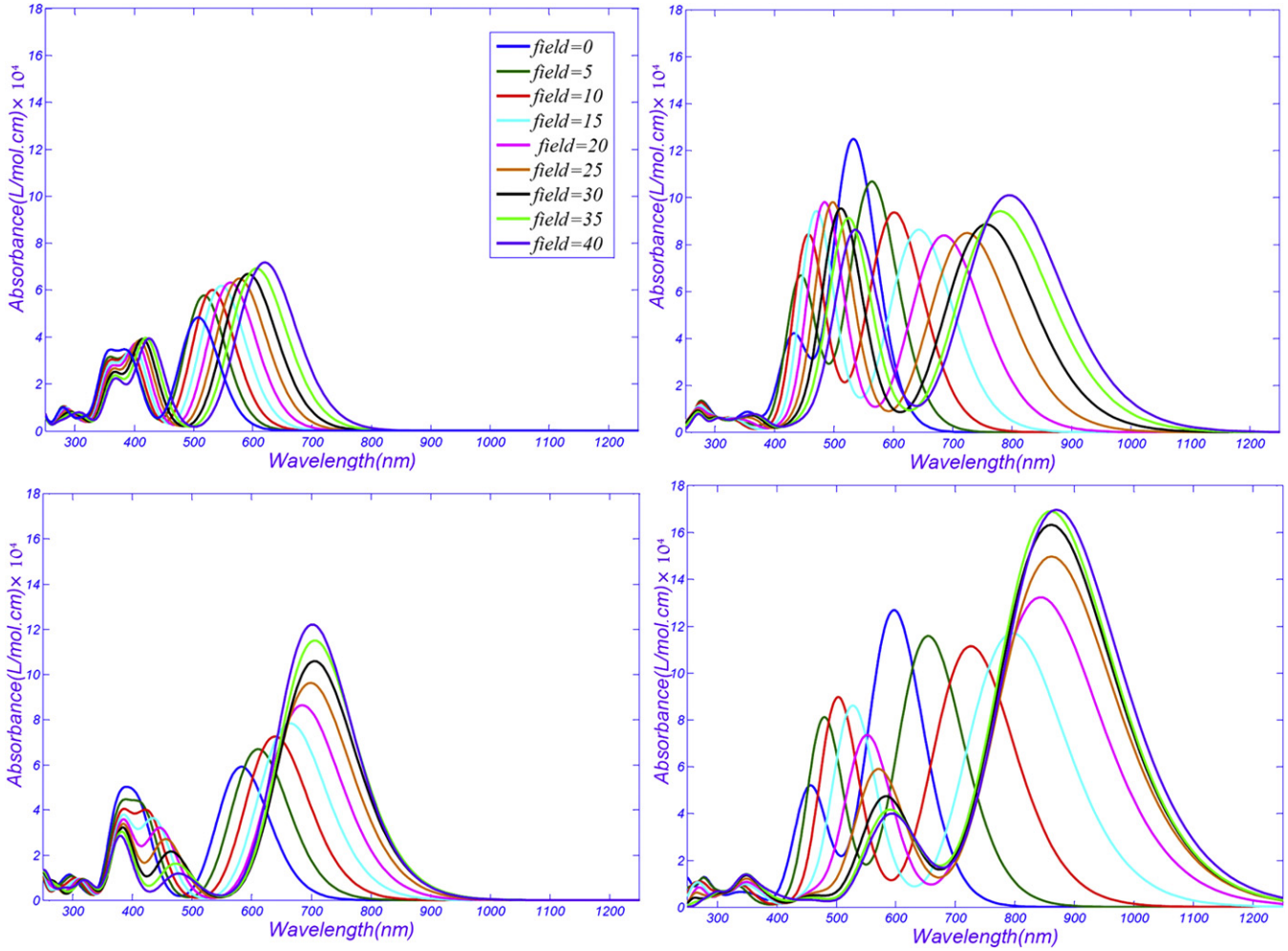

Fig. 5. Simulated absorption spectra of NKX-2593 (top) and NKX-2883 (bottom) in the gas phase (right) and ethanol solution (left), in various field ($\times 10^{-4}$ a.u.) strengths, calculated by TD-DFT at the MPW1PW91/6-311G (d) levels.

In this equation, the Peak Area for NKX-2593 in the gas phase and absence of a local field is selected to serve as an *A*-reference (A_{ref}) for MPW1PW91 and B3LYP, and *A* equals to Peak Area for the dyes in different field strengths in gas and solvent phases. As it is observable from the data in Table 4, the Peak Area is increased with increasing field strength, which is a result of peak broadening. The NKX-2883 bearing higher degree of resonance than NKX-2593 (because of extra cyanide and thiophene moieties) gets more affected from electric field and consequently undergoes more red-shift and increased Peak Area.

The results for MPW1PW91 and B3LYP are listed in Table 4. A simple comparison between MPW1PW91 and B3LYP methods reveals that the trend of changes for different conditions in both of them is similar. There is not a significant difference between the results obtained from MPW1PW91 and B3LYP, so B3LYP can also be used to calculate the Peak Area.

As mentioned previously, as a result of electric field application on NKX-2883, in spite of the shift to higher wavelengths, their oscillator strength is decreased for the electric field strength smaller than 20 a.u., but calculations show that in spite of the weakening of

Table 4
Numerical values for Peak Area for NKX-2593 and NKX-2883 in gas and solvent phases, in the presence of different fields ($\times 10^{-4}$ a.u.), calculated by TD-DFT and two hybrids functional MPW1PW91 and B3LYP/6-311G (d).

Field	Gas phase				Ethanol solution			
	NKX-2593		NKX-2883		NKX-2593		NKX-2883	
	MPW1PW91	B3LYP	MPW1PW91	B3LYP	MPW1PW91	B3LYP	MPW1PW91	B3LYP
0	0	0	108.15	108.47	50.48	51.62	167.32	169.29
5	11.36	11.30	123.16	123.70	72.43	73.35	221.11	224.56
10	19.43	19.28	142.07	142.88	94.10	94.68	282.32	287.06
15	27.84	27.58	165.5	166.70	116.70	125.88	362.16	366.81
20	36.23	35.78	193.3	194.53	141.73	137.49	448.90	447.38
25	45.07	44.39	224.63	225.12	167.32	160.81	514.04	503.82
30	54.60	53.56	257.72	255.71	188.02	179.56	544.88	529.99
35	64.77	69.40	290.19	285.78	202.87	193.004	556.03	539.78
40	75.19	72.89	319.54	312.08	210.65	210.04	569.14	551.51

oscillator strength, Peak Area, which is a criterion of light response of the dye to the solar spectrum, is increased. So, we can conclude that electric field application can lead to higher photon to current response of the dye.

To computationally study the absorption properties of the dyes using the TD-DFT method, our data suggest that Peak Area calculation method is more accurate and precise than the maximum absorption method because it covers all excited state transitions, even low intensity transitions, and also more vivid data about broadening of the peaks can be obtained using this method. Besides, by the use of Peak Area calculations, a comparison of the absorption properties of the dyes as well as their quantitative study would be possible. This method can be helpful for the analysis of the systems of similar absorption spectra.

Our data show that a field application in the proper direction can lead to a considerable change in efficiency improvement and red-shift. It is to be noted that an electric field application does not necessarily lead to higher efficiency, but a field of optimum strength and right direction is needed to do so.

4. Conclusions

The results of this work suggest that the DFT/TD-DFT approach is reliable for describing the electronic structure and spectral properties of Coumarin sensitizers, which can be of great help in the design of new and more efficient sensitizers for future-generation DSSCs. The electronic and spectroscopic properties of NKX-2593 and NKX-2883 Coumarin dyes have been investigated and compared with previous experimental works. Compared with experimental data, the results of the calculations imply that the hybrid functional PBE1PBE and MPW1PW91 are more suitable than B3LYP for calculating maximum absorption spectra of Coumarin dyes NKX-2593 and NKX-2883. Inclusion of solvent effects increases the oscillator strength significantly and results in red shifts of the spectra of NKX-2593 and NKX-2883. TD-DFT can be an appropriate method to calculate maximum absorption and oscillator strength. So, new structures can be suggested and we can then theoretically investigate how maximum absorption and oscillator strength increase can affect their efficiency. This paper describes a method to calculate electrostatic properties of excited states of molecular systems using time-dependent density functional theory in combination with a local electric field. Orientation of dyes in local electric field is one of the most important factors in applying an electric field on the dye. The results obtained from TD-DFT calculations indicate that the application of an electric field parallel to the dipole moment of the dye results in an incredible increase in the dipole moment of the dye, consequently influencing the absorption spectra. But the application of a local electric field anti-parallel to the orientation of the dipole moment of these two sensitizers resulted in a decrease in the dipole moment, compared to the off-field condition, and consequently blue-shifted the maximum absorption. According to these results, local fields parallel to the dipole moment of the dyes are in favor of our goal to promote the efficiency of the dyes in dye sensitizer solar cells.

We notice that the trend of calculated HOMO–LUMO gaps is nicely in accord with the spectroscopic data, showing a red-shift of the absorption maximum in going from NKX-2593 to NKX-2883. The NBO second order perturbation analysis provides a direct insight into the π-conjugation strength of NKX-2593 and NKX-2883. As it can be easily observed, as a result of the introduction of CN and thiophene to the dye NKX-2883 there is an increased resonance and stabilization in the molecule, verified by QMRE corresponding to second order perturbation. Peak Area calculation suggests that this method is more accurate and precise than the maximum absorption method because it covers all excited state transitions, even low intensity transitions, and also more vivid data about broadening of the peaks can be obtained using this method.

Changing the dye structure by introducing various functional groups to increase delocalization, and hence DSSCs' efficiency, is reported in a lot of studies. Our results indicate that the same improvement can be simply achieved by applying an electric field of proper strength and also show that electric field application to increase the photon-to-current power conversion of dye is very promising to provide good performances in dye sensitizer solar cell.

Acknowledgement

We would like to thank Dr. Sabzyan for providing us with hardware and software facilities.

Appendix A. Supplementary data

Supplementary data associated with this article can be found, in the online version, at doi:10.1016/j.jphotochem.2011.10.004.

References

[1] B. O'Regan, M. Grätzel, A low-cost, high-efficiency solar cell based on dye-sensitized colloidal TiO_2 films, Nature 353 (1991) 737–740.
[2] M. Grätzel, Conversion of sunlight to electric power by nanocrystalline dye-sensitized solar cells, J. Photochem. Photobiol. A 164 (2004) 3–14.
[3] M.K. Nazeeruddin, C. Klein, P. Liska, M. Grätzel, Synthesis of novel ruthenium sensitizers and their application in dye-sensitized solar cells, Coord. Chem. Rev. 249 (2005) 1460–1467.
[4] J. Bisquert, D. Cahen, G. Hodes, S. Rühle, A. Zaban, Physical chemical principles of photovoltaic conversion with nanoparticulate, mesoporous dye-sensitized solar cells, J. Phys. Chem. B 108 (2004) 8106–8118.
[5] H. Imahori, T. Umeyama, S. Ito, Large π-aromatic molecules as potential sensitizers for highly efficient dye-sensitized solar cells, Acc. Chem. Res. 42 (2009) 1809–1818.
[6] M.K. Nazeeruddin, S.M. Zakeeruddin, R. Humphry-Baker, M. Jirousek, P. Liska, N. Vlachopoulos, V. Shklover, C.-H. Fischer, M. Grätzel, Acid–base equilibria of (2,2′-bipyridyl-4,4′-dicarboxylic acid)ruthenium(II) complexes and the effect of protonation on charge-transfer sensitization of nanocrystalline titania, Inorg. Chem. 38 (1999) 6298–6305.
[7] H. Lindström, A. Holmberg, E. Magnusson, S.-E. Lindquist, L. Malmqvist, A. Hagfeldt, A new method for manufacturing nanostructured electrodes on plastic substrates, Nano Lett. 1 (2001) 97–100.
[8] M. Grätzel, Solar energy conversion by dye-sensitized photovoltaic cells, Inorg. Chem. 44 (2005) 6841–6851.
[9] M.K. Nazeeruddin, F. De Angelis, S. Fantacci, A. Selloni, G. Viscardi, P. Liska, S. Ito, B. Takeru, M. Grätzel, Combined experimental and DFT–TDDFT computational study of photoelectrochemical cell ruthenium sensitizers, J. Am. Chem. Soc. 127 (2005) 16835–16847.
[10] M.K. Nazeeruddin, Q. Wang, L. Cevey, V. Aranyos, P. Liska, E. Figgemeier, C. Klein, N. Hirata, S. Koops, S.A. Haque, J.R. Durrant, A. Hagfeldt, A.B.P. Lever, M. Grätzel, DFT-INDO/S modeling of new high molar extinction coefficient charge-transfer sensitizers for solar cell applications, Inorg. Chem. 45 (2005) 787–797.
[11] S. Kim, J.K. Lee, S.O. Kang, J. Ko, J.H. Yum, S. Fantacci, F. De Angelis, D. Di Censo, M.K. Nazeeruddin, M. Grätzel, Molecular engineering of organic sensitizers for solar cell applications, J. Am. Chem. Soc. 128 (2006) 16701–16707.
[12] A. Mishra, M.K.R. Fischer, P. Bäuerle, Metal-free organic dyes for dye-sensitized solar cells: from structure property relationships to design rules, Angew. Chem. Int. Ed. 48 (2009) 2474–2499.
[13] N. Koumura, Z.-S. Wang, S. Mori, M. Miyashita, E. Suzuki, K. Hara, Alkyl-functionalized organic dyes for efficient molecular photovoltaics, J. Am. Chem. Soc. 128 (2006) 14256–14257.
[14] R.C. White, J.E. Benedetti, A.D. Gonçalves, W. Romão, B.G. Vaz, M.N. Eberlin, C.R.D. Correia, M.A. De Paoli, A.F. Nogueira, Synthesis, characterization and introduction of a new ion-coordinating ruthenium sensitizer dye in quasi-solid state TiO_2 solar cells, J. Photochem. Photobiol. A 222 (2011) 185–191.
[15] Y. Pellegrin, L. Le Pleux, E. Blart, A. Renaud, B. Chavillon, N. Szuwarski, M. Boujtita, L. Cario, S. Jobic, D. Jacquemin, F. Odobel, Ruthenium polypyridine complexes as sensitizers in NiO based p-type dye-sensitized solar cells: effects of the anchoring groups, J. Photochem. Photobiol. A 219 (2011) 235–242.
[16] R. Sivakumar, A.T.M. Marcelis, S. Anandan, Synthesis and characterization of novel heteroleptic ruthenium sensitizer for nanocrystalline dye-sensitized solar cells, J. Photochem. Photobiol. A 208 (2009) 154–158.
[17] M. Liang, W. Xu, F. Cai, P. Chen, B. Peng, J. Chen, Z. Li, New triphenylamine-based organic dyes for efficient dye-sensitized solar cells, J. Phys. Chem. C 111 (2007) 4465–4472.
[18] W. Xu, B. Peng, J. Chen, M. Liang, F. Cai, New triphenylamine-based dyes for dye-sensitized solar cells, J. Phys. Chem. C 112 (2008) 874–880.

[19] T. Horiuchi, H. Miura, K. Sumioka, S. Uchida, High efficiency of dye-sensitized solar cells based on metal-free indoline dyes, J. Am. Chem. Soc. 126 (2004) 12218–12219.
[20] D.P. Hagberg, T. Edvinsson, T. Marinado, G. Boschloo, A. Hagfeldt, L. Sun, A novel organic chromophore for dye-sensitized nanostructured solar cells, Chem. Commun. (2006) 2245–2247.
[21] S. Ito, S.M. Zakeeruddin, R. Humphry-Baker, P. Liska, R. Charvet, P. Comte, M.K. Nazeeruddin, P. Péchy, M. Takata, H. Miura, S. Uchida, M. Grätzel, High-efficiency organic-dye-sensitized solar cells controlled by nanocrystalline-TiO_2 electrode thickness, Adv. Mater. 18 (2006) 1202–1205.
[22] D. Kim, C. Kim, H. Choi, K. Song, M.-S. Kang, J. Ko, A new class of organic sensitizers with fused planar triphenylamine for nanocrystalline dye sensitized solar cells, J. Photochem. Photobiol. A 219 (2011) 122–131.
[23] G. Zhang, H. Bala, Y. Cheng, D. Shi, X. Lv, Q. Yu, P. Wang, High efficiency and stable dye-sensitized solar cells with an organic chromophore featuring a binary π-conjugated spacer, Chem. Commun. (2009) 2198–2200.
[24] S. Hwang, J.H. Lee, C. Park, H. Lee, C. Kim, C. Park, M.-H. Lee, W. Lee, J. Park, K. Kim, N.-G. Park, C. Kim, A highly efficient organic sensitizer for dye-sensitized solar cells, Chem. Commun. (2007) 4887–4889.
[25] Y. Kurashige, T. Nakajima, S. Kurashige, K. Hirao, Y. Nishikitani, Theoretical investigation of the excited states of coumarin dyes for dye-sensitized solar cells, J. Phys. Chem. A 111 (2007) 5544–5548.
[26] K. Hara, T. Sato, R. Katoh, A. Furube, Y. Ohga, A. Shinpo, S. Suga, K. Sayama, H. Sugihara, H. Arakawa, Molecular design of coumarin dyes for efficient dye-sensitized solar cells, J. Phys. Chem. B 107 (2002) 597–606.
[27] K. Hara, M. Kurashige, S. Ito, A. Shinpo, S. Suga, K. Sayama, H. Arakawa, Novel polyene dyes for highly efficient dye-sensitized solar cells, Chem. Commun. (2003) 252–253.
[28] K. Hara, Z.-S. Wang, T. Sato, A. Furube, R. Katoh, H. Sugihara, Y. Dan-oh, C. Kasada, A. Shinpo, S. Suga, Oligothiophene-containing coumarin dyes for efficient dye-sensitized solar cells, J. Phys. Chem. B 109 (2005) 15476–15482.
[29] K. Hara, K. Sayama, Y. Ohga, A. Shinpo, S. Suga, H. Arakawa, A coumarin-derivative dye sensitized nanocrystalline TiO solar cell having a high solar-energy conversion efficiency up to 5.6%, Chem. Commun. (2001) 569–570.
[30] Z.-S. Wang, Y. Cui, Y. Dan-oh, C. Kasada, A. Shinpo, K. Hara, Thiophene-functionalized coumarin dye for efficient dye-sensitized solar cells: electron lifetime improved by coadsorption of deoxycholic acid, J. Phys. Chem. C 111 (2007) 7224–7230.
[31] H. Kohjiro, W. Zhong-Sheng, K. Nagatoshi, S. Kazuhiro, Efficient organic-dye-sensitized nanocrystalline TiO_2 solar cells, in: IEEE 4th World Conference, 2006, pp. 313–316.
[32] Z.-S. Wang, K. Hara, Y. Dan-oh, C. Kasada, A. Shinpo, S. Suga, H. Arakawa, H. Sugihara, Photophysical and (photo)electrochemical properties of a coumarin dye, J. Phys. Chem. B 109 (2005) 3907–3914.
[33] K. Hara, M. Kurashige, Y. Dan-oh, C. Kasada, A. Shinpo, S. Suga, K. Sayama, H. Arakawa, Design of new coumarin dyes having thiophene moieties for highly efficient organic-dye-sensitized solar cells, New J. Chem. 27 (2003) 783–785.
[34] Z.-S. Wang, Y. Cui, Y. Dan-oh, C. Kasada, A. Shinpo, K. Hara, Molecular design of coumarin dyes for stable and efficient organic dye-sensitized solar cells, J. Phys. Chem. C 112 (2008) 17011–17017.
[35] H. Kusama, H. Sugihara, Theoretical study of quinolines–I_2 intermolecular interaction and implications on dye-sensitized solar cell performance, J. Comput. Chem. 26 (2005) 1372–1382.
[36] X.-H. Zhang, C. Li, W.-B. Wang, X.-X. Cheng, X.-S. Wang, B.-W. Zhang, Photophysical, electrochemical, and photoelectrochemical properties of new azulene-based dye molecules, J. Mater. Chem. 17 (2007) 642–649.
[37] H.-J. Koo, K. Kim, N.-G. Park, S. Hwang, C. Park, C. Kim, Fabrication of heterosensitizer-junction dye-sensitized solar cells, Appl. Phys. Lett. 92 (2008) 142103.
[38] B. Miehlich, A. Savin, H. Stoll, H. Preuss, Results obtained with the correlation energy density functionals of becke and Lee, Yang and Parr, Chem. Phys. Lett. 157 (1989) 200–206.
[39] A.D. Becke, A new mixing of Hartree–Fock and local density-functional theories, J. Chem. Phys. 98 (1993) 1372–1377.
[40] M. Cossi, V. Barone, R. Cammi, J. Tomasi, Ab initio study of solvated molecules: a new implementation of the polarizable continuum model, Chem. Phys. Lett. 255 (1996) 327–335.
[41] A.D. Becke, Density-functional thermochemistry. III. The role of exact exchange, J. Chem. Phys. 98 (1993) 5648–5652.
[42] R.E. Stratmann, G.E. Scuseria, M.J. Frisch, An efficient implementation of time-dependent density-functional theory for the calculation of excitation energies of large molecules, J. Chem. Phys. 109 (1998) 8218–8224.
[43] M.E. Casida, C. Jamorski, K.C. Casida, D.R. Salahub, Molecular excitation energies to high-lying bound states from time-dependent density-functional response theory: characterization and correction of the time-dependent local density approximation ionization threshold, J. Chem. Phys. 108 (1998) 4439–4449.
[44] C.-P. Hsu, S. Hirata, M. Head-Gordon, Excitation energies from time-dependent density functional theory for linear polyene oligomers: butadiene to decapentaene, J. Phys. Chem. A 105 (2000) 451–458.
[45] S. Hirata, M. Head-Gordon, Time-dependent density functional theory within the Tamm–Dancoff approximation, Chem. Phys. Lett. 314 (1999) 291–299.
[46] C. Adamo, V. Barone, Exchange functionals with improved long-range behavior and adiabatic connection methods without adjustable parameters: the MPW and MPW1PW models, J. Chem. Phys. 108 (1998) 664–675.
[47] F.J. Luque, J.M. López, M. Orozco, Perspective on "Electrostatic interactions of a solute with a continuum. A direct utilization of ab initio molecular potentials for the prevision of solvent effects", Theor. Chem. Acc.: Theor. Comput. Model. (Theor. Chim. Acta) 103 (2000) 343–345.
[48] M.J.T. Frisch, G.W. Trucks, H.B. Schlegel, G.E. Scuseria, M.A. Robb, J.R. Cheeseman Jr., T. Vreven, K.N. Kudin, J.C. Burant, S.S. Iyengar, J. Tomasi, V. Barone, B.C. Mennucci, G. Scalmani, N. Rega, G.A. Petersson, H.H. Nakatsuji, M. Ehara, K. Toyota, R. Fukuda, J. Hasegawa, M. Ishida, T. Nakajima, Y. Honda, Y. Kitao, O. Nakai, M. Klene, X. Li, J.E. Knox, J.B. Cross, V. Bakken, C. Adamo, J. Jaramillo, R. Gomperts, R.E. Stratmann, O. Yazyev, A.J. Austin, R. Cammi, C. Pomelli, J.W. Ochterski, P.Y. Ayala, K. Morokuma, G.A. Voth, P. Salvador, J.J. Dannenberg, V.G. Zakrzewski, S. Dapprich, A.D. Daniels, O. Farkas, D.K. Malick, A.D. Rabuck, K.F. Raghavachari, Ö. Farkas, J.V. Ortiz, Q. Cui, A.G. Baboul, S.C. Clifford, J. Stefanov, B.B. Liu, G. Liashenko, A. Piskorz, I.M.P. Komaromi, R.L. Fox, D.J. Keith, T. Al-Laham, C.Y.N. Peng, A. Challacombe, M. Gill, P.M.W. Johnson, W.W.B. Chen, M.W. Gonzalez, J.A. Pople, Gaussian 03, I.P. Revision D.01, Gaussian, PA, 2003.
[49] E.D. Glendening, J.K. Badenhoop, A.E. Reed, J.E. Carpenter, J.A. Bohmann, C.M. Morales, F. Weinhold, NBO5.0; Theoretical, U.o.W.M. Chemistry Institute, WI, 2001.
[50] H.-W. Xi, K.H. Lim, Theoretical study of germabutadienic internal rotations and π-conjugation, Organometallics 27 (2008) 5748–5758.
[51] H. Kusama, H. Sugihara, K. Sayama, Simultaneous interactions of Ru dye with iodide ions and nitrogen-containing heterocycles in dye-sensitized solar cells, J. Phys. Chem. C 114 (2010) 11335–11341.
[52] S. Ghosh, G.K. Chaitanya, K. Bhanuprakash, M.K. Nazeeruddin, M. Grätzel, P.Y. Reddy, Electronic structures and absorption spectra of linkage isomers of trithiocyanato (4,4′,4″ tricarboxy-2,2′:6,2′-terpyridine) ruthenium(II) complexes: a DFT study, Inorg. Chem. 45 (2006) 7600–7611.
[53] F. De Angelis, S. Fantacci, A. Selloni, Time-dependent density functional theory study of the absorption spectrum of [Ru(4,4′-COOH-2,2′-bpy)$_2$(NCS)$_2$] in water solution: influence of the pH, Chem. Phys. Lett. 389 (2004) 204–208.
[54] S.I. Gorelsky, SWizard Program, Version 4.6, University of Ottawa, Ottawa, 2010, http://www.sg-chem.net/swizard.
[55] R.J. Cave, K. Burke, E.W. Castner, Theoretical investigation of the ground and excited states of coumarin 151 and coumarin 120, J. Phys. Chem. A 106 (2002) 9294–9305.
[56] D.H. Oh, S.G. Boxer, Stark effect spectra of Ru(diimine)$_3^{2+}$ complexes, J. Am. Chem. Soc. 111 (1989) 1130–1131.
[57] S. Ardo, Y. Sun, A. Staniszewski, F.N. Castellano, G.J. Meyer, Stark effects after excited-state interfacial electron transfer at sensitized TiO_2 nanocrystallites, J. Am. Chem. Soc. 132 (2010) 6696–6709.
[58] S. Ardo, Y. Sun, F.N. Castellano, G.J. Meyer, Excited-state electron transfer from ruthenium-polypyridyl compounds to anatase TiO_2 nanocrystallites: evidence for a Stark effect, J. Phys. Chem. B 114 (2010) 14596–14604.
[59] U.B. Cappel, S.M. Feldt, J. Schöneboom, A. Hagfeldt, G. Boschloo, The influence of local electric fields on photoinduced absorption in dye-sensitized solar cells, J. Am. Chem. Soc. 132 (2010) 9096–9101.
[60] D. Gosztola, H. Yamada, M.R. Wasielewski, Electric field effects of photogenerated ion pairs on nearby molecules: a model for the carotenoid band shift in photosynthesis, J. Am. Chem. Soc. 117 (1995) 2041–2048.
[61] M. Ponder, R. Mathies, Excited-state polarizabilities and dipole moments of diphenylpolyenes and retinal, J. Phys. Chem. 87 (1983) 5090–5098.
[62] F.C. Grozema, R. Telesca, H.T. Jonkman, L.D.A. Siebbeles, J.G. Snijders, Excited state polarizabilities of conjugated molecules calculated using time dependent density functional theory, J. Chem. Phys. 115 (2001) 10014–10021.
[63] S.G. Boxer, Stark realities, J. Phys. Chem. B 113 (2009) 2972–2983.
[64] A. Hinchliffe, H.J. Soscún, Ab initio studies of the dipole moment and polarizability of azulene in its ground and excited singlet states, Chem. Phys. Lett. 412 (2005) 365–368.